AUTOMATED NEAR REAL TIME RADARSAT-2 IMAGE GEO-PROCESSING AND ITS APPLICATION FOR SEA ICE AND OIL SPILL MONITORING

Ziqiang Ou

Canadian Ice Service, Environment Canada
373 Sussex Drive, Ottawa, Canada K1A 0H3 - Ziqiang.Ou@ec.gc.ca

KEY WORDS: RADARSAT, SAR, Georeferencing, Real-time, Pollution, Snow Ice, Detection

ABSTRACT:

Synthetic aperture radar (SAR) data from RADARSAT-1 are an important operational data source for several ice centres around the world. Sea ice monitoring has been the most successful real-time operational application for RADARSAT-1 data. These data are used by several national ice services as a mainstay of their programs. Most recently, Canadian Ice Service launched another new real-time operational program called ISTOP (Integrated Satellite Tracking Of Pollution). It uses the RADARSAT-1 data to monitor ocean and lakes for oil slicks and tracking the polluters. In this paper, we consider the ice information requirements for operational sea ice monitoring and the oil slick and target detection requirements for operational ISTOP program at the Canadian Ice Service (CIS), and the potential for RADARSAT-2 to meet those requirements. Primary parameters are ice-edge location, ice concentration, and stage of development; secondary parameters include leads, ice thickness, ice topography and roughness, ice decay, and snow properties. Iceberg detection is an additional ice information requirement. The oil slick and ship target detection are the basic requirements for the surveillance and pollution control.

1. INTRODUCTION

RADARSAT-2 products are provided in a GeoTIFF format with a sets of support XML files for all products except the RAW. The GeoTIFF images are georeferenced, but not geocorrected so that they are not ready for most of GIS and Remote Sensing applications, which require the RADARSAT-2 images being overlaid with other geographic data layers. Since the products are not geographically corrected, the geographic metadata included in GeoTIFF is limited to a set of points tying image location to geographic location. GeoTIFF images is generated in TIFF strip format. Multipolar images is generated as separate GeoTIFF image files. All images are oriented such that north is nominally up and east is nominally on the right. Further processing is required in order to integrate the dataset into CIS existing operational Integrated Spatial Information System – ISIS (Ou, 2004; Koonar et al. 2004) and the Integrated Satellite Tracking Of Pollution – ISTOP system (Gauthier et al. 2007).

Both ISIS for ice monitoring and ISTOP for oil monitoring are real-time or near real-time applications. The data acquisition and the data processing time is one of the critical factors. Considering the data volume of SAR images and in order to meet the time requirements, an automated and fast SAR image processing and geo-referencing algorithm is the key for the success of both applications. Thus, this paper will discuss the automated fast RADARSAT-2 image geo-processing by using the image geographical tie points provided in the RADARSAT-2 product; the evaluation of geographical location accuracy for the geocoded image; the evaluation of image geo-spatial distortion introduced by geo-processing and how to minimize the distortion and improve the image's geo-location accuracy. A set of different geo-reference procedures will be evaluated based on their spatial accuracy of geocoded image and their computational efficiencies in order to meet the requirements for the mapping accuracy of ice and oil and the time constraint of these real-time applications.

2. GEOMETRIC TRANSFORMATION

There are two major techniques for correcting geometric distortion present in an image. The first is to model the nature and magnitude of the sources of distortion and then use these models to correct for distortions. The second is to establish a mathematical relationship between the locations of pixels in an image (X,Y) and their location (U,V) in the real world (e.g. on a map). The latter is by far the most common, though many standard sources of satellite images will have at least some corrections done by modelling before the user receives the data.

The idea is to develop a mathematical function that relates the image and real world coordinate systems. e.g. X = f(U, V) and Y = g(U, V). While in the end we want to transform our images in the pixel coordinate system into some coordinate system in the real world, in actuality this is accomplished in reverse. Once a real world coordinate system is established, the mapping functions (f, g) are used to determine which pixels in the image whose centers fall closest to the locations of the real-world grid.

The transformation from a image coordinate system to a real world coordinate system through a set of tie points of the two coordinate systems can be mathematically expressed by a set of mapping functions with respect to two coordinate components. The coordinate mapping from any point [u, v] in the image coordinate system to the corresponding point [x, y] in the real world coordinate system is modelled as:

$$x = f(u, v \,/\, \alpha)$$
$$y = g(u, v \,/\, \beta)$$

$$(1)$$

where α and β are parameters of the mapping function f and g respectively and are determined by control points, and are commonly determined by a global transformation.

Since the 2D polynomial functions do not reflect the sources of distortion during the image formation and do not correct for terrain relief distortions, they are limited to images with few or small distortions, such as nadir-viewing images, systematically-corrected images and/or small images over flat terrain. These functions correct for local distortions at the ground control point (GCP) location. They are very sensitive to input errors and hence GCPs have to be numerous and regularly distributed. Consequently, these functions should not be used when precise geometric positioning is required for multi-source multi-format data integration and in high relief areas. If a second order polynomial function is used, the following is obtained:

$$x = \alpha_0 + \alpha_1 u + \alpha_2 v + \alpha_3 uv + \alpha_4 u^2 + \alpha_5 v^2$$
$$y = \beta_0 + \beta_1 u + \beta_2 v + \beta_3 uv + \beta_4 u^2 + \beta_5 v^2 \quad (2)$$

From a mathematical point of view, a first order polynomial transformation requires a minimum of 3 points, a second order polynomial requires a minimum of 6 points and, a third order polynomial requires a minimum of 10 points. Generally, if the order of polynomial model is n, we must at least have a set of M=(n+1)(n+2)/2 GCPs to solve Equations (1). Suppose that $\{(u_i, v_i): i = 1, \ldots, n\}$ and $\{(x_i, y_i): i=1, \ldots, n\}$ are the tying GCP pairs from image and real world coordinate systems respectively, we can form n equations for both x and y as following:

$$x_i = \alpha_0 + \alpha_1 u_i + \alpha_2 v_i + \alpha_3 u_i v_i + \alpha_4 u_i^2 + \alpha_5 v_i^2 + \varepsilon_{x_i}$$
$$y_i = \beta_0 + \beta_1 u_i + \beta_2 v_i + \beta_3 u_i v_i + \beta_4 u_i^2 + \beta_5 v_i^2 + \varepsilon_{y_i}$$
$$(3)$$

By assuming that the ε are independent and identically distributed (iid) observation errors, i.e.,

$$\varepsilon = \begin{bmatrix} \varepsilon_x \\ \varepsilon_y \end{bmatrix}, \quad \varepsilon \sim N \left\{ \begin{bmatrix} 0 \\ 0 \end{bmatrix}, \begin{bmatrix} \sigma_x^2 & 0 \\ 0 & \sigma_y^2 \end{bmatrix} \right\} \quad (4)$$

the equations constructed from the GCPs by (3) could be separated into two sets of equations as shown in (5) below,

$$X = WA + \varepsilon_x$$
$$Y = WB + \varepsilon_y \quad (5)$$

where

$$\varepsilon_x = \begin{bmatrix} \varepsilon_{x_1} \\ \varepsilon_{x_2} \\ \vdots \\ \varepsilon_{x_n} \end{bmatrix}, \quad \varepsilon_y = \begin{bmatrix} \varepsilon_{y_1} \\ \varepsilon_{y_2} \\ \vdots \\ \varepsilon_{y_n} \end{bmatrix}, \quad A = \begin{bmatrix} \alpha_0 \\ \alpha_1 \\ \alpha_2 \\ \alpha_3 \\ \alpha_4 \\ \alpha_5 \end{bmatrix}, \quad B = \begin{bmatrix} \beta_0 \\ \beta_1 \\ \beta_2 \\ \beta_3 \\ \beta_4 \\ \beta_5 \end{bmatrix}$$

$$W = \begin{bmatrix} 1 & u_1 & v_1 & u_1 v_1 & u_1^2 & v_1^2 \\ 1 & u_2 & v_2 & u_2 v_2 & u_2^2 & v_2^2 \\ \vdots & \vdots & \vdots & \vdots & \vdots & \vdots \\ 1 & u_n & v_n & u_n v_n & u_n^2 & v_n^2 \end{bmatrix}$$

$$X = \begin{bmatrix} x_1 \\ x_2 \\ \vdots \\ x_n \end{bmatrix}, \quad Y = \begin{bmatrix} y_1 \\ y_2 \\ \vdots \\ y_n \end{bmatrix}$$

This means that the two sets of coefficients α_j and β_j could be estimated separately. The least square estimation can be used to determine the coefficients of α_j and β_j from GCPs.

$$Min[\varepsilon_x^T \varepsilon_x] = (W\hat{A} - X)^T (W\hat{A} - X)$$
$$Min[\varepsilon_y^T \varepsilon_y] = (W\hat{B} - Y)^T (W\hat{B} - Y) \quad (6)$$

These are two standard least square problems. The estimation for α_j and β_j are in Equation (7).

$$\hat{A} = (W^T W)^{-1} W^T X$$
$$\hat{B} = (W^T W)^{-1} W^T Y \quad (7)$$

The corresponding variance components estimation (Ou, 1989) are in Equation (8).

$$\hat{\sigma}_x^2 = \tfrac{1}{n-r} (W\hat{A} - X)^T (W\hat{A} - X)$$
$$\hat{\sigma}_y^2 = \tfrac{1}{n-r} (W\hat{B} - Y)^T (W\hat{B} - Y) \quad (8)$$

where r = rank(W). Thus, the transformation functions f and g are determined. The total variance could be estimated by:

$$\hat{\sigma}_t^2 = \hat{\sigma}_x^2 + \hat{\sigma}_y^2 \quad (9)$$

Sometimes we also need to determine the inverse transformation of Equation (1) from the GCPs set, which transforms the coordinate from (x_i, y_i) to (u_i, v_i).

$$u = f^{-1}(x, y / \alpha')$$
$$v = g^{-1}(x, y / \beta')$$

(10)

The same procedure could be used to estimate the coefficients α'_j and β'_j of transformation (10).

There are many challenges presented by global transformations that require consideration here. For global transformation models such as affine transformation, projective transformation, and global polynomial transformation, the parameters α and β are the same for all the points and are determined by all the control points, so a single function is used to model the transformation for each component of coordinates. When the geometric distortion is complex and location dependent, global models become inadequate to model the image geometry. Linear functions such as affine transformation and projective transformation are too simple to take the local variation into consideration. Nonlinear functions such as global polynomials use the least square methods to optimize the parameters, thus the local variation will be averaged across the whole image (Zitova and Flusser, 2003). Consequently, the registration error of locally deformed images by global functions is usually large and the spatial distribution of the error also varies with the location.

3. RADARSAT-2 IMAGE GEOPROCESSING

The basic product as generated by the RADARSAT-2 processor contains a Product Information File and one or more Image Pixel Data Files. The composition of RADARSAT-2 products is shown in Figure 1. All RADARSAT-2 products include one or more Image Pixel Data Files. One, two, or four Image Pixel Data Files may be included, corresponding to single, dual, or quad polarization modes, respectively. Each file contains the raster SAR image for a given polarization in GeoTIFF format (MDA, 2003).
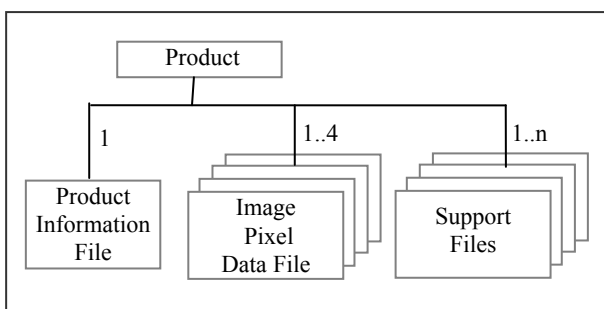
Figure 1: Product Composition

The Product Information File is an ASCII file that logically groups known information on the product. For example, groupings are provided for source, image generation and imagery information related to the product. The Product Information File is encoded in Extensible Markup Language (XML) format as shown in Figure 2.

All products (except RAW) are georeferenced, but not geocorrected. Since these products are not geographically corrected, the geographic metadata included in GeoTIFF is limited to the four corners tying image location to geographic location. GeoTIFF images are generated in TIFF strip format. Multi-polar images will be generated as separate GeoTIFF image files. All images are oriented such that north is nominally up and east is nominally on the right.

A grid of tie points is included in the product.xml under the **geolocationGrid** node (highlighted in Figure 2), which ties the line/pixel positions in image coordinates to geographical latitude/longitude. The image coordinates are in units of pixels. The ground coordinates are latitude and longitude in units of decimal degrees. The ground coordinates are referenced to WGS-84, and pixel and line numbers start at 0. These grid tie points are used as Ground Control Points (GCP) to automatically geo-correct the image.
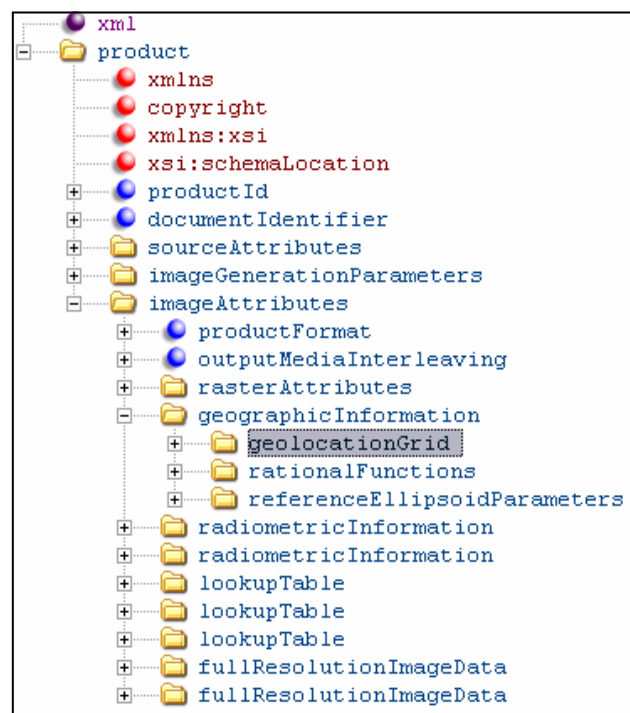
Figure 2: RADARSAT-2 Product XML Node Tree

The Figure 3 and Figure 4 below give an example of RADARSAT-2 ScanSAR Wide dataset with image size of 10508×10039 and pixel spacing and line spacing of 50 meters. The Figure 3 shows the GCP distribution in image coordinates and Figure 4 shows the GCP distribution in geographic coordinates. The GCPs are evenly distributed across the whole image.
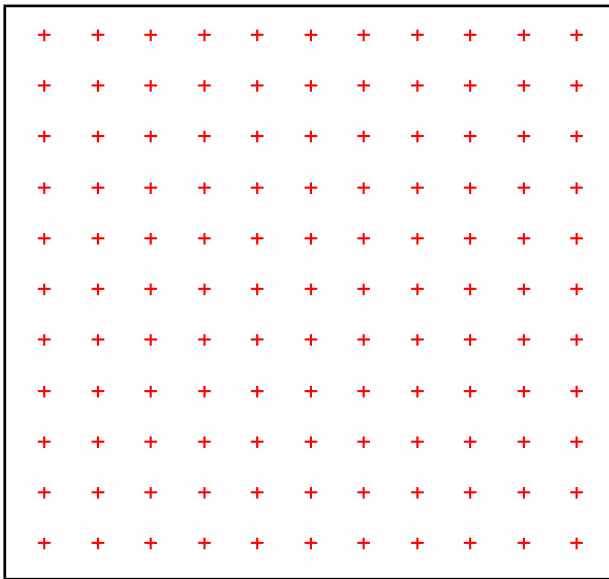
Figure 3: Sample of RADARSAT-2 GCPs Distribution in Image Coordinate System

First, the geographic latitude and longitude of GCPs are projected onto a planar map coordinate system. In our case, we use Polar Stereographic (PS) projection for high arctic region and Lambert Conformal Conic (LCC) for the rest of Canada. Then, a global polynomial transformation Equation (2) between the image coordinates (pixel/line) and the projected map coordinates is determined through the least square regression.
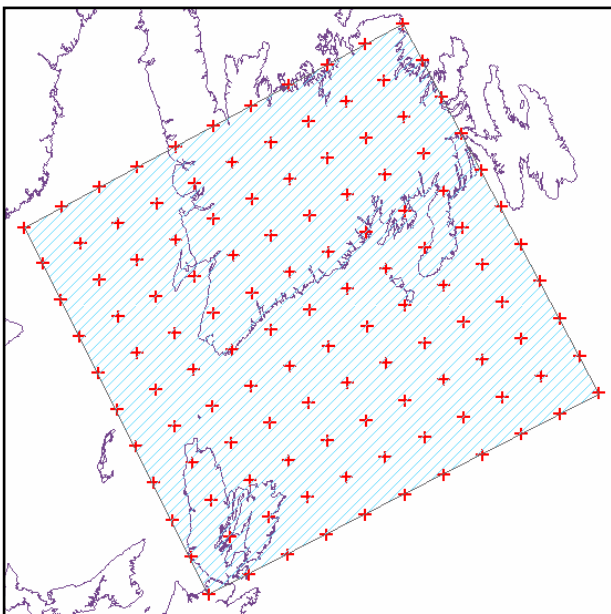
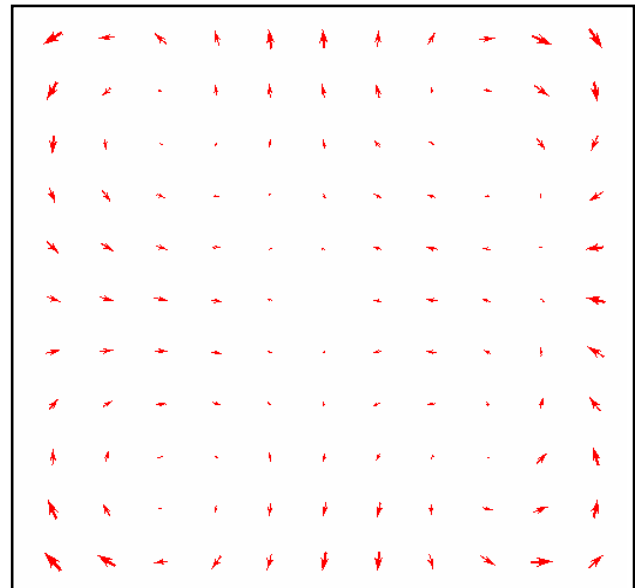

Figure 4: GCPs Geographic Distribution

Figure 5: Total Errors for a 2nd Order Global Polynomial Transformation (RMS: 0.96 Pixel)

In most cast, a perfect fit for all GCPs would require an unnecessarily high order of transformation. Instead of increasing the order, the user has option to tolerate a certain amount of error. When the transformation coefficients of the global polynomial transformation equation (1) and its the inverse transformation (10) are calculated, the inverse transformation (10) is used to retransform the reference coordinates of the GCPs back to the source coordinate system. Unless the order of transformation allows for a perfect fit, there is some discrepancy between the source coordinates and the retransformed reference coordinates. The Figure 5 displays the discrepancies at all GCP locations for the example in Figure 3. It clearly shows that the errors along the image edges are larger than the centre of the image.

The Root Mean Square (RMS) error is the average distance between the input source location of all GCPs and their retransformed locations. They can be estimated based on equation (8) and (9). The discrepancies shown in Figure 5 are enlarged for presentation purpose. The actual values are estimated as below.

$$\hat{\sigma}_x = 0.66, \quad \hat{\sigma}_y = 0.70 \quad \text{and} \quad \hat{\sigma}_t = 0.96 \qquad (11)$$

The estimated total RMS error is 0.96 pixel, which is smaller than 1 pixel. This indicates that a second order global transformation polynomial is good enough for our ice and oil spill monitoring applications. The **geolocationGrid** tie points (GCPs) provided in product.xml will be used to automatically geo-correct the RADARSAT-2 images. The diagram in Figure 6 shows the automated data processing flow.
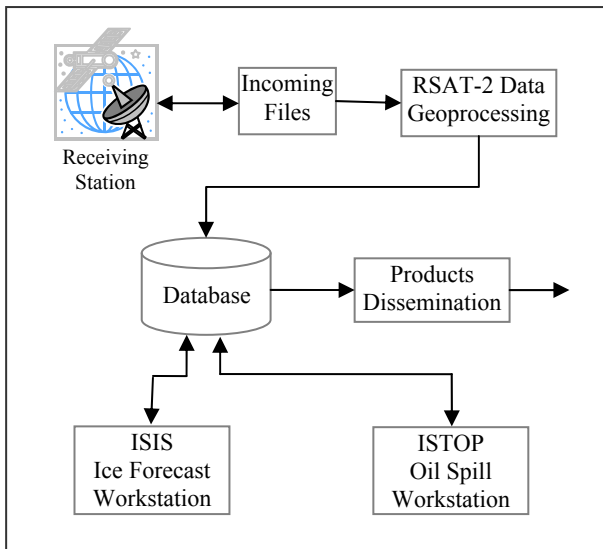
Figure 6: Data Processing Flow Diagram

| Co-Polarization Channel: VV | Cross-Polarization Channel: VH |

Figure 7: Co-Polarization vs Cross-Polarization at High Wind Condition

4. ICE APPLICATIONS

Comparing to RADARSAT-1 single polarization SAR data, RADARSAT-2 is capable of acquiring dual-polarization and fully polarimetric SAR data. The RADARSAT-2 dual-polarization options include HH–HV or VV–VH modes. The additional information provided by the cross-polarization channel could be very useful, as the cross polarization channel responds to different scattering mechanisms than the co-polarization channel (Scheuchl et al. 2004). These dual-polarization data are available in all beam configurations, giving a wide choice in resolution, coverage, and incidence angle. Most importantly, dual polarization is available in ScanSAR modes, which are mostly used for ice and oil monitoring at CIS from RADARSAT-1 data. Operational experience by CIS analysts results in a preference of HH over VV for co-polarization channels.

The cross-polarization HV and VH backscatter response from water are generally low and are relatively independent of wind-induced surface roughness conditions, whereas their backscatter from sea ice are affected by surface roughness, volume scattering, and multi-bounce scattering. Thus, the ice–ocean contrast of cross-polarization can be expected to be greater than that for either of the co-polarization channels, especially at high wind conditions as shown in Figure 7. The cross-polarization data can enhance the structural information of sea ice and have demonstrated some utility for improving discrimination between smooth and deformed ice as well. The combined use of co-polarization and cross-polarization channel will give better results across a wider range of incidence angles.
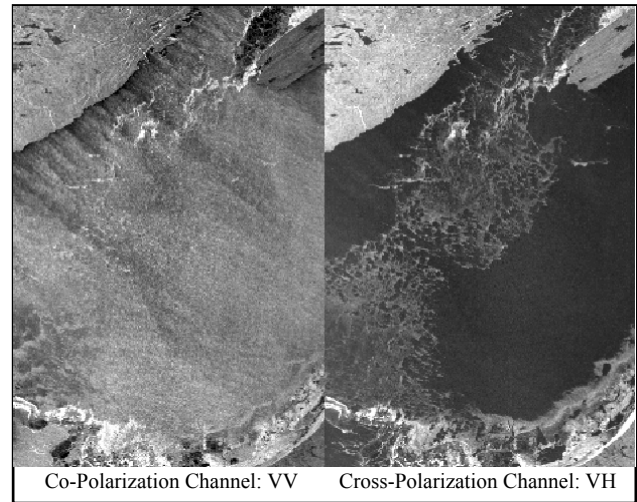
5. OIL SPILL APPLICATIONS

CIS is an important partner to Canada's NASP (National Aerial Surveillance Program) by using earth observation technology (RADARSAT imagery) to look for oil-like signatures (anomalies) on the ocean's surface that could be indicative of an oil spill. The CIS operational ISTOP (Integrated Satellite Tracking of Pollution) program currently uses RADARSAT-1 ScanSAR HH polarization data to identify potential oil spills, to track ship targets (Gauthier et al. 2007), and to direct pollution surveillance flights to the locations of potential pollution incidents.

The SAR signal is sensitive to the roughness of the sea surface, which is modulated by wind speed and direction; imagery acquired at VV polarization is the most sensitive to wind speed variability (as shown in Figure 7). The suppression of the capillary waves by oil from either anthropogenic sources, such as an oil spill, or from natural biological slicks, reduces the surface roughness resulting in less radar backscatter and darker image tones. The detection of oil slicks has been found to be best in moderate wind conditions in the range of 3 to 10 m/s.

Although imagery in both VV and HH polarizations from RADARSAT-2 can be used for slick detection, the VV imagery might be preferred as, in general, it offers a better signal to clutter ratio than other polarization choices (i.e., HH, VH, or HV). Although VV is more sensitive than HH for slick detection, there may not be any advantage to using the co-polarized or cross-polarized signatures as oil-free and oil-covered surfaces tend to have similar contrast and polarization ratios. Slick thickness and the inability to differentiate oil slicks from "look-alikes" such as areas of low-wind, grease ice, or biological surfactants remain problematic.

One of CIS research priority is to assess the utility of RADARSAT-2 VV/VH dual channel ScanSAR data for the ISTOP program. It is known that VV polarization provides superior CNR for oil detection over HH polarization. On the other hand, VV is less appropriate for ship detection. However, VH polarization has shown promise in detecting ships (figure 3)[2]. ISTOP will be working with others to investigate more fully whether the VH channel of RADARSAT-2 can perform

adequately for ship detection. If so, VV/VH will be likely replace HH as the default ISTOP acquisition mode (DeAbreu et al. 2006).

REFERENCES

DeAbreu, R., Gauthier, M.F., and Wychen, W.V., 2006. SAR-Based Oil Pollution Surveillance in Canada: Operational Implementation and Research Priorities, *Proceedings OceanSAR 2006 – Third Workshop on Coastal and Marine Applications of SAR*, St. John's, NL, Canada, October 2006.

Gauthier, M. F., Weir, L., Ou, Z., Arkett, M. and DeAbreu, R., 2007. Integrated Satellite Tracking of Pollution – A New Operational Program, *International Geoscience and Remote Sensing Symposium (IGARSS),* July 2007, Barcelona, Spain.

Koonar, A., Ou, Z., and Scarlett, B. 2004. A real-time geo-spatial information system: an integration of GIS technologies for ice forecasting, *Advances in Spatial Analysis and Decision Making*, 2004 Swets & Zeitlinger, Lisse, ISBN:9058096521, pp.221-227

MDA, 2003. RADARSAT-2 Product Format Definition, RN-RP-51-2713 Issue 1/5: NOV. 24, 2003

Ou, Z., 1989. Estimation of variance and covariance components, *Bulletin Geodesique*, Vol.63, p.139-148.

Ou, Z., 2004. An Integrated Spatial Information System for Ice Service, *The 20th Congress of International Society of Photogrammetry and Remote Sensing (ISPRS)* at Istanbul, Turkey.

Scheuchl, B., Flett, D., Ron Caves, R. and Cumming, I., 2004. Potential of RADARSAT-2 data for operational sea ice monitoring, *Canadian Journal of Remote Sensing*, Vol. 30, No. 3, pp. 448–461

Zitova, B. and Flusser, J., 2003, Image registration methods: a survey, *Image and Vision Computing*, 21(11): 977-1000.